Electronic Supplementary Information for

Direct Observation of Electrically Degenerate Interface Layer in GaN/Sapphire Heterostructure

Young-Min Kim,*‡[ab] Sung Bo Lee,‡[c] Jaekwang Lee*[d] and Sang Ho Oh*[a]

This file includes:

Supplementary Note 1

Figures S1–S14

[a] Department of Energy Science, Sungkyunkwan University (SKKU), Suwon 16419, Republic of Korea. E-mail: youngmk@skku.edu, sanghooh@skku.edu
[b] Center for Integrated Nanostructure Physics, Institute for Basic Science (IBS), Suwon 16419, Republic of Korea.
[c] Department of Materials Science and Engineering and Research Institute of Advanced Materials (RIAM), Seoul National University, Seoul 08826, Republic of Korea.
[d] Department of Physics, Pusan National University, Busan 46241, Republic of Korea. E-mail: jaekwangl@pusan.ac.kr
‡ Equal contribution.

Supplementary Note 1. Geometrical phase analysis for strain mapping

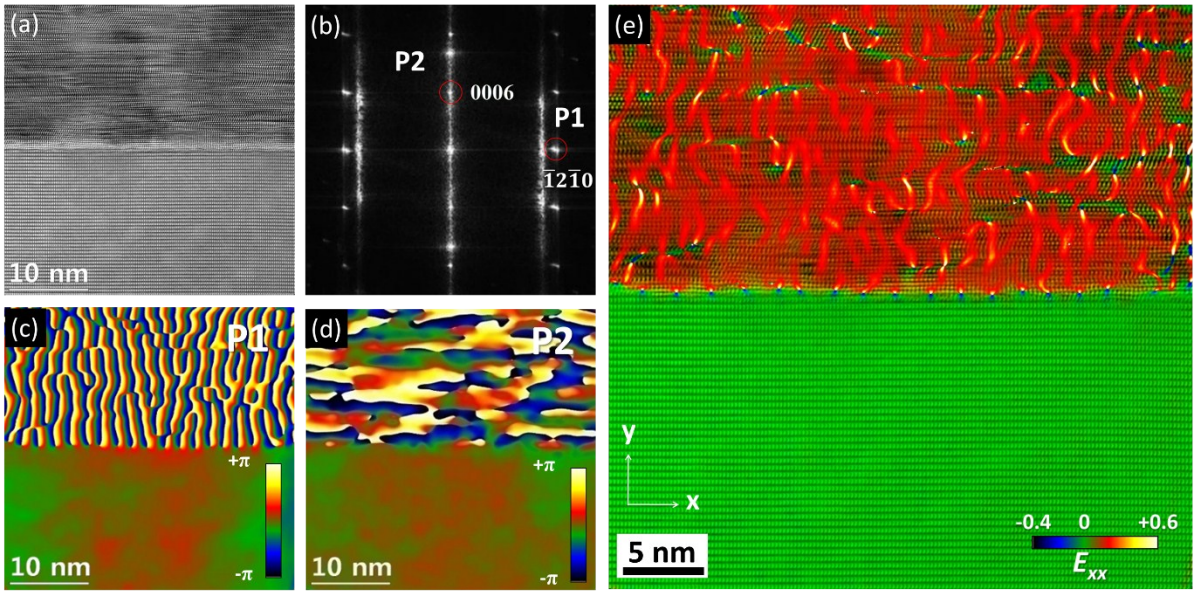

Figure S1. Geometrical phase analysis (GPA) to resolve the array of the in-plane misfit dislocations at GaN/sapphire interface. (a) A representative HRTEM image of GaN/sapphire heterointerface. (b) Fast Fourier transform (FFT) of the HRTEM image. $(\bar{1}2\bar{1}0)$ and (0006) Bragg reflections of the sapphire substrate, which are marked as circles P1 and P2, respectively, are used for calculating the respective geometric phase images (c) and (d). The colored scale bar shows a normalized phase variation from –π to +π. (e) The in-plane strain (E_{xx}) map calculated from the phase images, P1 and P2. For clear spatial visualization of the correspondence between the HRTEM and the strain map, each image is superimposed. The color scale indicates the magnitude of the in-plane strain relative to the sapphire reference area. Note that the strain artifact due to the optical distortions introduced by the microscope itself was characterized and corrected by measuring the local displacement fields from HRTEM images of an unstrained, perfect crystalline Au sample.

The two-dimensional displacement fields, $u(r)$, can be measured by analyzing noncolinear Fourier components of the lattice fringes, g_1 and g_2, in an HRTEM image as a routine of GPA. The resulting phase images, $P_{g1}(r)$ and $P_{g2}(r)$, are simply related to the displacement field by the relation,

$$u(r) = -\frac{1}{2\pi}\left[P_{g1}(r)a_1 + P_{g2}(r)a_2\right]$$

where a_1 and a_2 are the real-space lattice vectors for g_1 and g_2, respectively [Hÿtch *et al.*, *Ultramicroscopy* **1998**, 74, 131; Chung *et al.*, *Nat. Commun.* **2015**, 6, 8252]. Therefore, the

phase images describe the position of the lattice fringes in real space with respect to a reference because any displacement of the lattice fringes will result in a phase shift. An in-plane strain map, E_{xx}, with respect to the sapphire reference can be derived from differentiation of the displacement field, *u(r)*, with the relation of $E_{xx} = {\partial u(x)}/{\partial x}$ as shown in Fig. S1. The calculated in-plane strain map was superimposed on the HRTEM image to highlight the defective nature of the interface region (Fig. S1e). The spatial resolution depends on the mask size and the precision is a direct function of the noise level in the GPA analysis. We used the mask size of 0.89 1/nm to select in-plane and out-of-plane lattice vector components, P1 and P2 (Fig. S1b). This size is translated into 1.21 nm as a spatial resolution. In the resulting in-plane strain map (Fig. S1e), we estimated the measurement precision to be ± 0.49 %. When increasing the mask size, the spatial resolution is improved but the precision becomes worse. It is generally recommended that one can select a mask size of g/2 as a maximum.

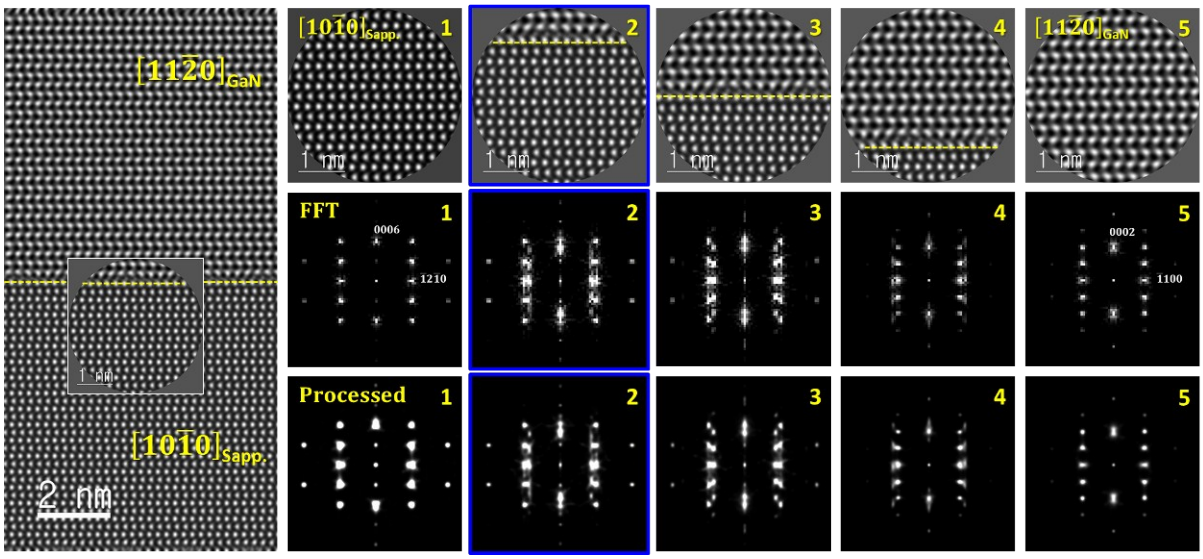

Figure S2. Local FFT analysis for the simulated HRTEM image shown in Figure 1b. The image window used for the analysis is 3.75 (w) × 3.75 (h) nm^2 (see the inset in the large simulated HRTEM image). The series of local HRTEM images arranged in numerical order (1 to 5) in the first row were extracted from the region of sapphire substrate to the GaN region across the interface (yellow dotty line) in the large simulated HRTEM image. In the second row, FFT patterns corresponding to each local HRTEM image were displayed. For the local FFT, circular mask was applied to remove unwanted edge signal usually appeared in the resulting FFT pattern of square image. The array of FFT patterns shown in the last row were the results of the Richardson–Lucy deconvolution used for the experimental FFT results as shown in Figure 3. The simulated HRTEM image of the region 2 including three layers of GaN (outlined by blue box) is similar to the experimental HRTEM image of the region 3 shown in Figure 3. It is worthy to note that the FFT pattern of the region 2 simply shows a composite pattern of sapphire and GaN because the simulated model has a simple abrupt interface without the pseudomorphically strained layer just above sapphire substrate.

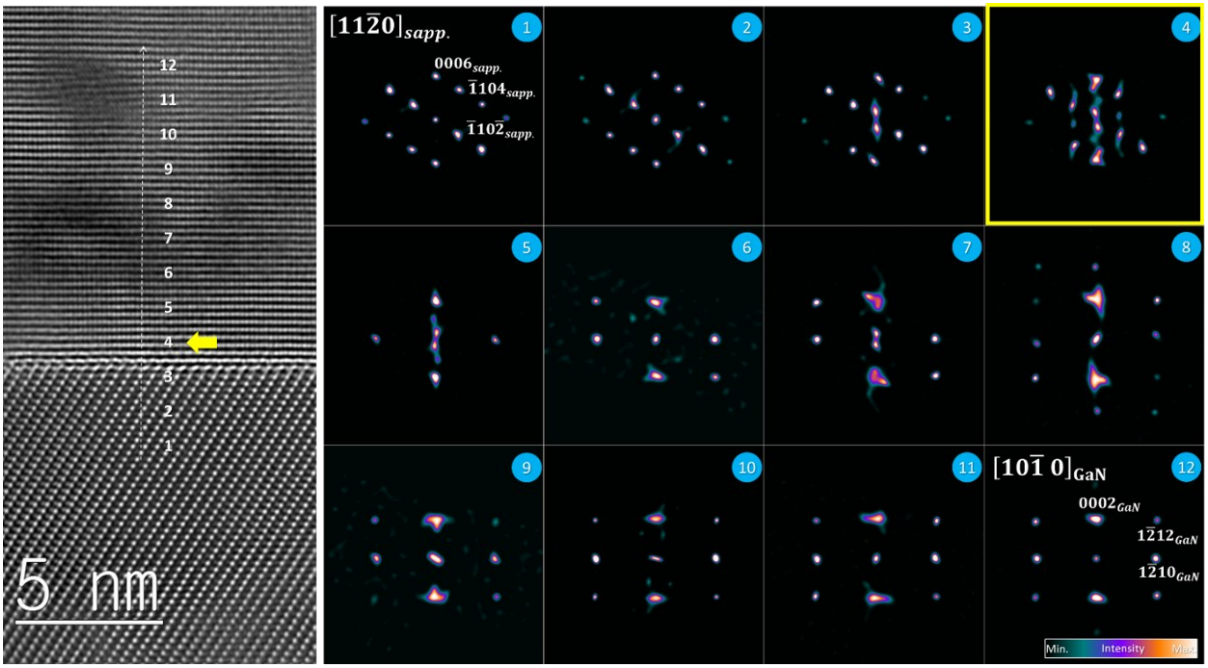

Figure S3. Extra series of local FFTs to show crystallographic structure changes across the interface. The left HRTEM image shows a high-resolution GaN/sapphire interface structure viewed at a 30° tilted angle of the sample shown in Fig. 1. The crystallographic orientation relationship between the substrate and film is $[10\bar{1}0]_{GaN} \parallel [11\bar{2}0]_{sapp.}$. The 12 FFT patterns of the magnified HRTEM images (not shown) acquired along the white dotted line across the interface were obtained with the same deconvolution process mentioned in this study.

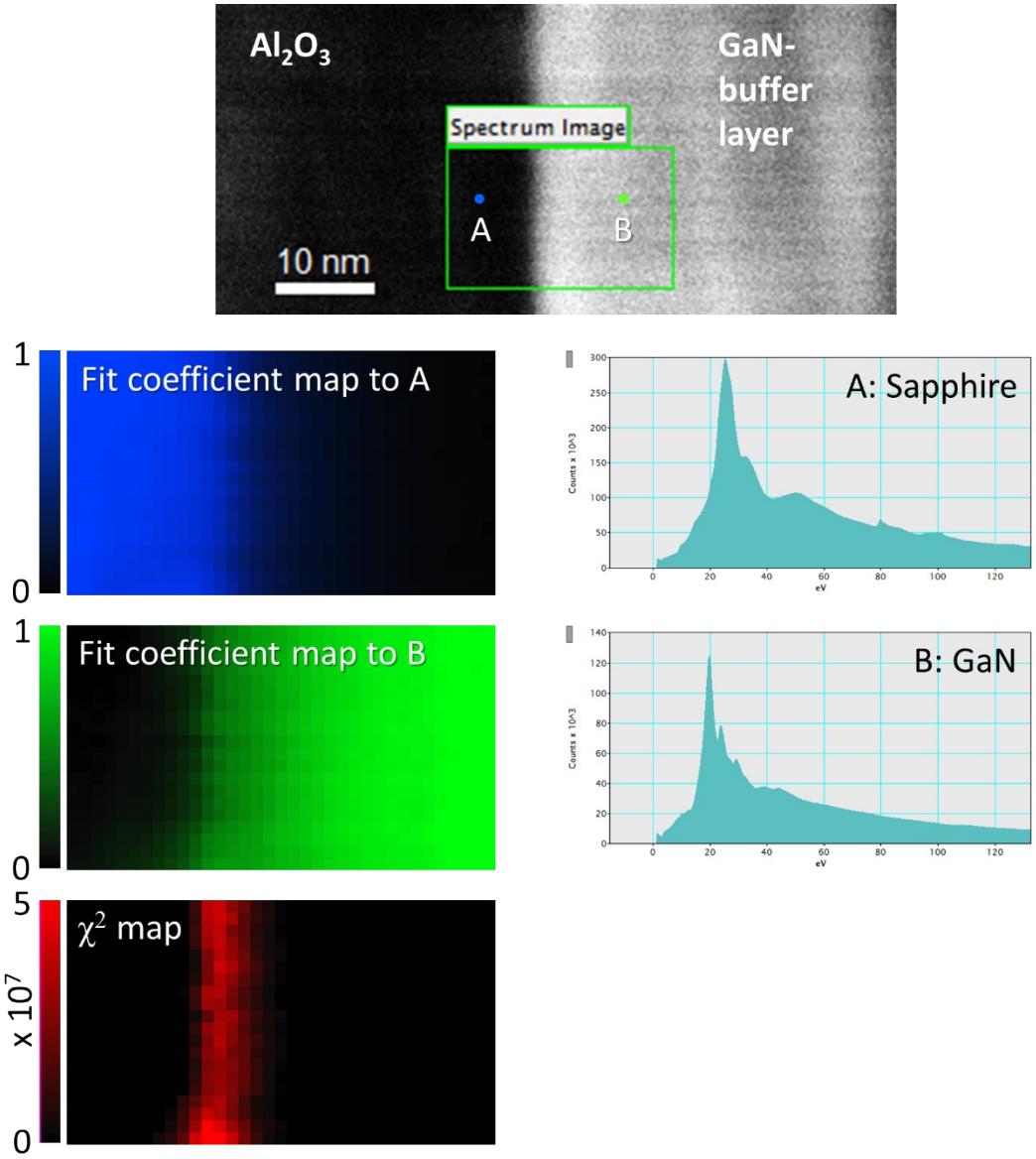

Figure S4. Results of MLLS fitting of the two low-loss spectra, A (sapphire, blue) and B (GaN, green) in the plasmonic energy range (5–35 eV). In this fitting method, the χ^2 map (red) represents deviation from the linear superposition of the local spectra, A and B [Borisevich *et al.*, *Phys. Rev. Lett.*, 2010, **105**, 087204]. We can observe anomalous residual signal along the interface region from the χ^2 map. This result supports that interphase phase dissimilar to sapphire and GaN exists at the interface region.

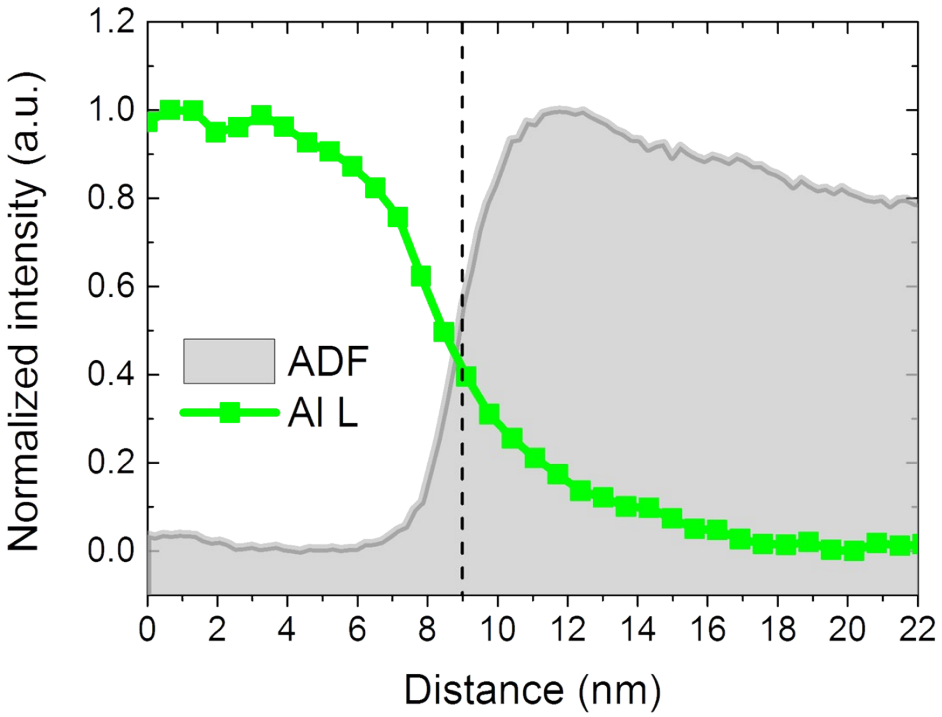

Figure S5. Intensity profile of the Al $L_{2,3}$ edge across the sapphire/GaN interface obtained from the low-loss EELS data shown in Fig. 4(a). Note that the large tail of Al L signal penetrated into GaN side is due to the unavoidable delocalization of EELS signals, which practically limits the successful EELS chemical analysis with high spatial resolution. Not like the intensities of O K and N K edges, Al L intensity much more suffers from the EELS signal delocalization (Muller and Silcox et al., Ultramicroscopy **1995**, 59, 195) because the extent of signal delocalization is strongly dependent on the energy loss; The energy loss dependence of it is given by b = hv/ΔE, where b, h, v, and ΔE are impact parameter, speed of incident electrons, Plank constant, and energy loss, respectively. Because Al L edge is found at ~80 eV, the EELS signal delocalization of the Al L edge would be 5 or 7 times larger than those of N and O K edges. Therefore, the long tail of Al L edge intensity does not mean the diffusion of Al into GaN. To investigate whether an element is mobile across the interface, the EELS signal profile should be compared with the simultaneously-acquired HAADF signal that shows the position of interface with higher spatial resolution. It is generally accepted that there is no discernable chemical mixing if the middle point of EELS elemental signal is well matched with that of HAADF intensity profile.

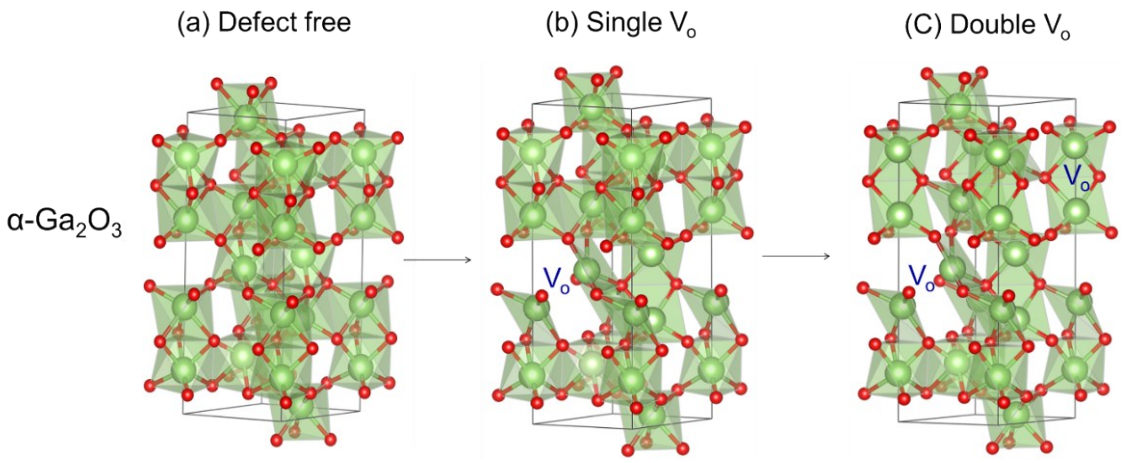

Figure S6. Atomic structures of (a) defect free α-Ga_2O_3, (b) α-Ga_2O_3 with single oxygen vacancy (V_o), and (c) α-Ga_2O_3 with double V_o.

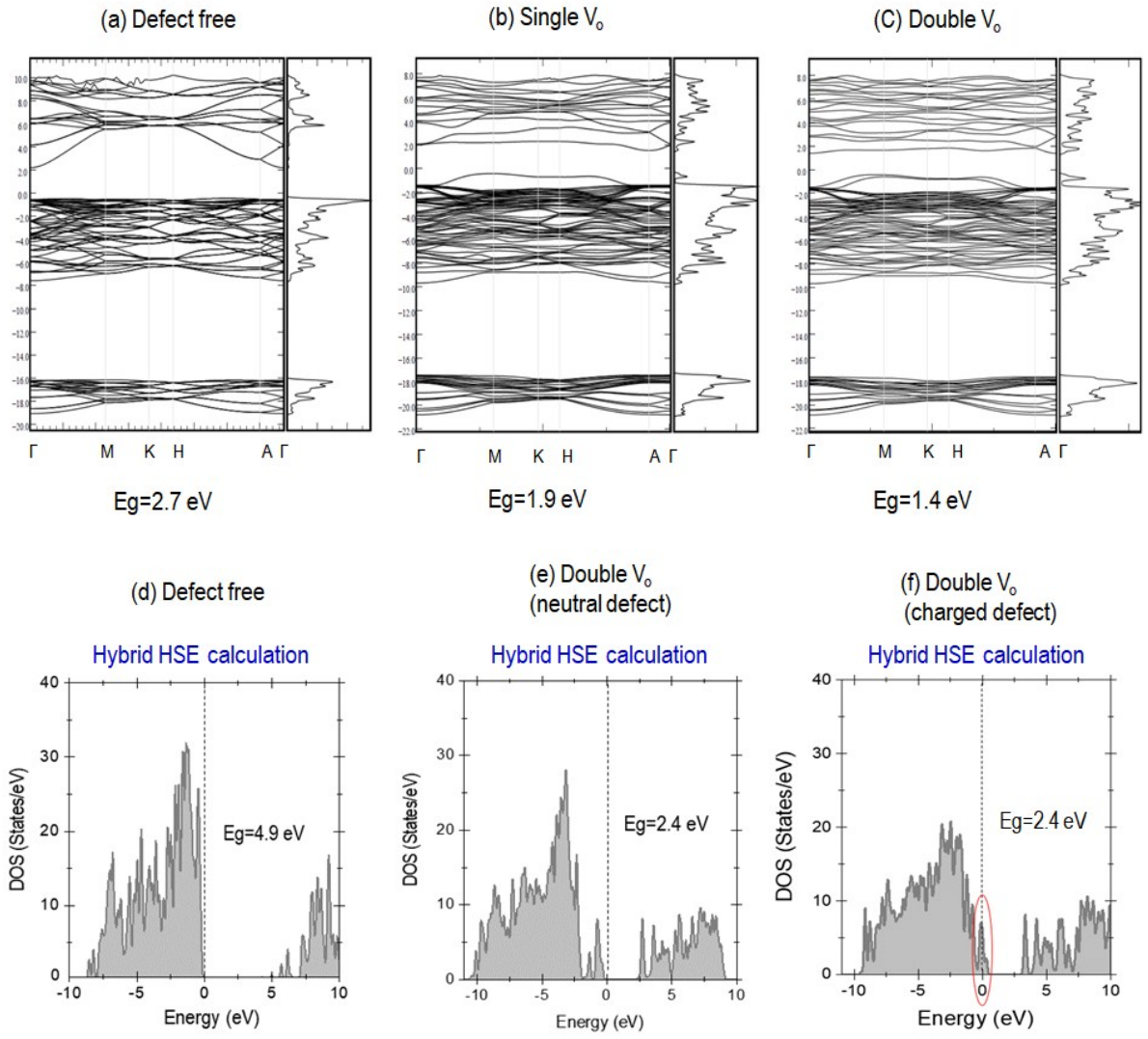

Figure S7. Electronic band structures and density of states of (a) defect free α-Ga_2O_3, (b) α-Ga_2O_3 with single oxygen vacancy (V_o), and (c) α-Ga_2O_3 with double V_o obtained by using conventional PBE functional. Density of states of (d) defect free α-Ga_2O_3, (e) α-Ga_2O_3 with neutral double V_o, and (f) α-Ga_2O_3 with charged double V_o obtained by using hybrid HSE functional. For the defect free bulk α-Ga_2O_3, electronic bandgap of 4.9 eV is obtained by using hybrid HSE functional, which is same to the experimental bandgap of 4.9 eV (Fig. S6 (d)). Therefore, HSE functional reproduces the electronic structure of α-Ga_2O_3 very well. For the defective α-Ga2O3 (with double oxygen vacancy), the bandgap is estimated to be about 2.4 eV using hybrid HSE functional (Fig. S6 (e)). We have considered a charged defect by removing one electron from defective α-Ga_2O_3, but there is no big change in band gap (Fig. S6 (f)). Accordingly, it is expected that the band offset between α-Ga_2O_3 conduction band and GaN valence band is still about 0.6 eV. As indicated in red circle, there exist a sharp state originated from charged defect near the wide valence band, it seems to be localized but connected to wide valence band at the tiny level. Accordingly, depending on the defect concentration, it can be delocalized.

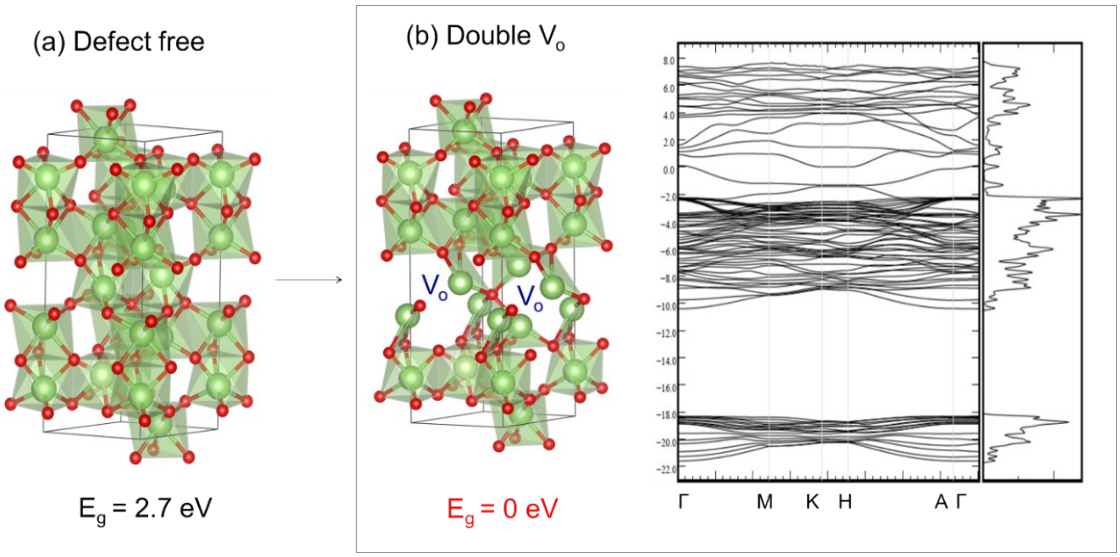

Figure S8. Atomic structure and electronic property of α-Ga_2O_3 with double V_o in the same plane.

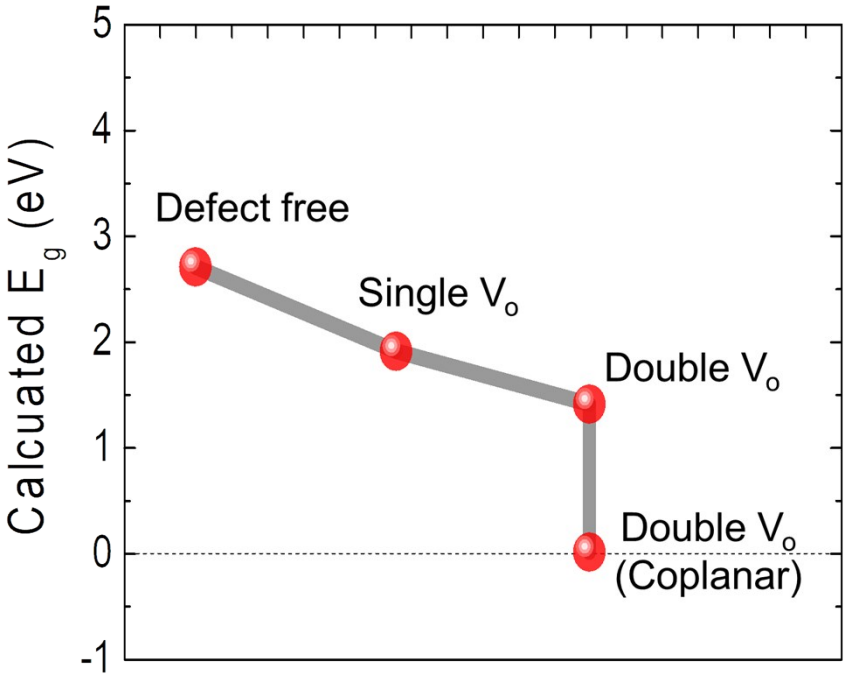

Figure S9. Bandgap change in bulk α-Ga_2O_3 depending on the oxygen vacancy concentration and its position. For the defective α-Ga_2O_3 calculations, one oxygen atom and two oxygen atoms were removed from the conventional unit cell of α-Ga_2O_3 composed of 12 Ga atoms and 18 O atoms, which corresponds to 5.6% and 11% vacancy concentrations, respectively. For the double vacancy calculations, two different configurations depending on the relative position of two oxygen vacancies as shown in Figure S6 and Figure S8 were considered. The band gap of α-Ga_2O_3 reduces almost linearly depending on the oxygen vacancy concentration

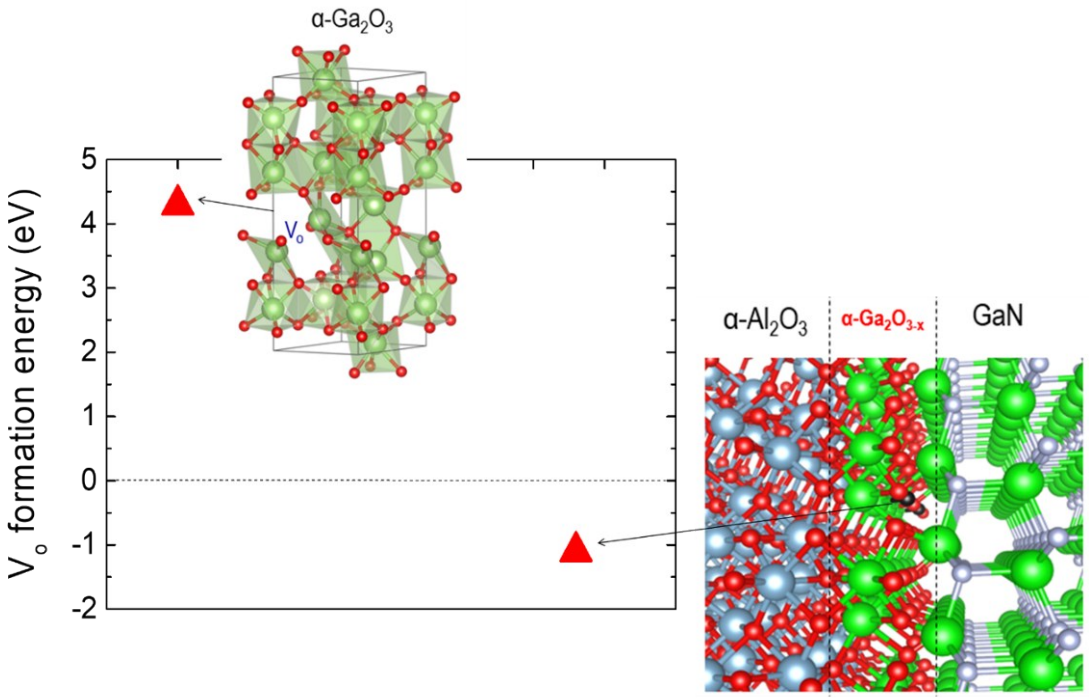

Figure S10. Oxygen vacancy formation energies in bulk α-Ga_2O_3 and interface degenerate layer. For the oxygen vacancy formation energy in bulk α-Ga_2O_3 and GaN/Al_2O_3 heterostructure containing interface, one oxygen atom is removed at the bulk α-Ga_2O_3 and GaN/Al_2O_3 heterostructure, respectively. For the bulk, an oxygen atom is removed at the supercell 6(Ga_2O_3) composed of 12 Ga and 36 Oxygen atoms. For the heterostructure containing interface, one oxygen atom is removed at the interface of GaN/Al_2O_3 heterostructure composed of 54 Ga, 54 N, 44 Al, 72 Oxygen atoms. The oxygen vacancy formation energy (E_f) was determined using the following formula: $E_f = E(Ga_{12}O_{17}) - E(Ga_{12}O_{18}) + (1/2)\ E(O_2\text{-molecule})$ for the bulk α-Ga_2O_3 and $E_f = E(Ga_{54}N_{54}Al_{44}O_{71}) - E(Ga_{54}N_{54}Al_{44}O_{72}) + (1/2)\ E(O_2\text{-molecule})$ for the heterostructure containing the interface, where $E(Ga_{12}O_{17})$ is the total energy of a supercell (6(Ga_2O_3)) containing single oxygen vacancy, $E(Ga_{12}O_{18})$ is the total energy of a perfect Ga_2O_3 in the same size of supercell, $E(O_2$-molecule) is the total energy of O_2 molecule. $E(Ga_{54}N_{54}Al_{44}O_{71})$ is the total energy of GaN/Al_2O_3 heterostructure containing single oxygen vacancy, $E(Ga_{54}N_{54}Al_{44}O_{72})$ is the total energy of GaN/Al_2O_3 heterostructure. Oxygen vacancy formation energy in GaN/Al_2O_3 heterostructure is estimated about negative 1.1 eV, which strongly indicates that oxygen vacancies in degenerate layer are formed spontaneously.

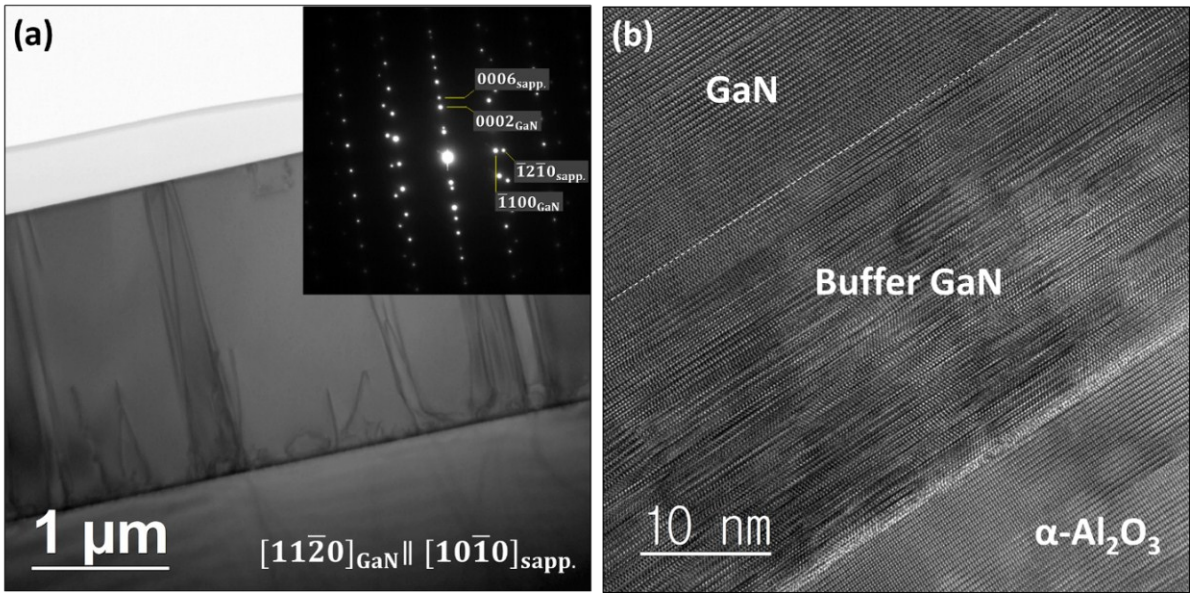

Figure S11. Microstructure of the GaN film grown on sapphire. (a) A bright-field TEM image of the GaN/sapphire heterostructure used in this study. Inset is the corresponding selected area diffraction pattern showing the crystallographic orientation relationship of $[11\bar{2}0]_{GaN} \parallel [10\bar{1}0]_{Sapp.}$ between the GaN film and sapphire substrate. (b) An HRTEM image of the interface region of the GaN/sapphire heterostructure. The buffer GaN film with a thickness of 25 nm was grown by employing the two-step growth method.

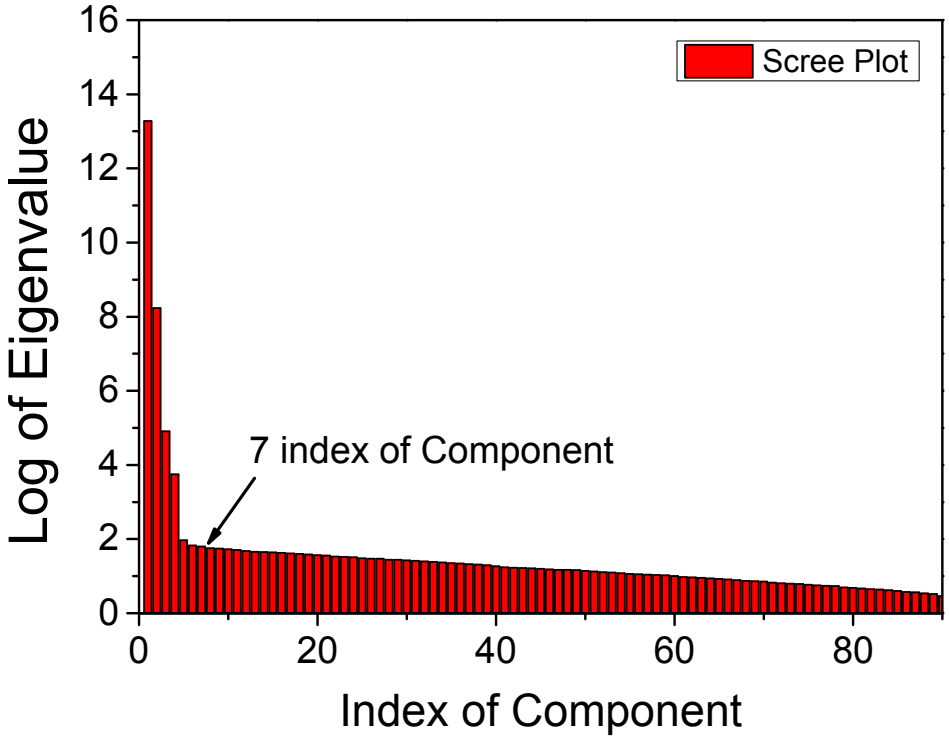

Figure S12. Scree plot of the PCA eigenvalues obtained from weighted PCA analysis of the core-loss spectrum image for O *K* and N *K* edges as shown in Figure 4d,e.

Parameter	Value
Acc. Voltage (keV)	1250
Spherical aberration coefficient (mm)	2.65
Chromatic aberration coefficient (mm)	4.1
Convergence semi-angle (mrad)	0.85
Defocus spread (nm)	30
Specimen drift (nm/sec)	0.1
y-axis vibration (nm)	0.05
Defocus (nm)	5 (overfocus)
Thickness (nm)	11.5

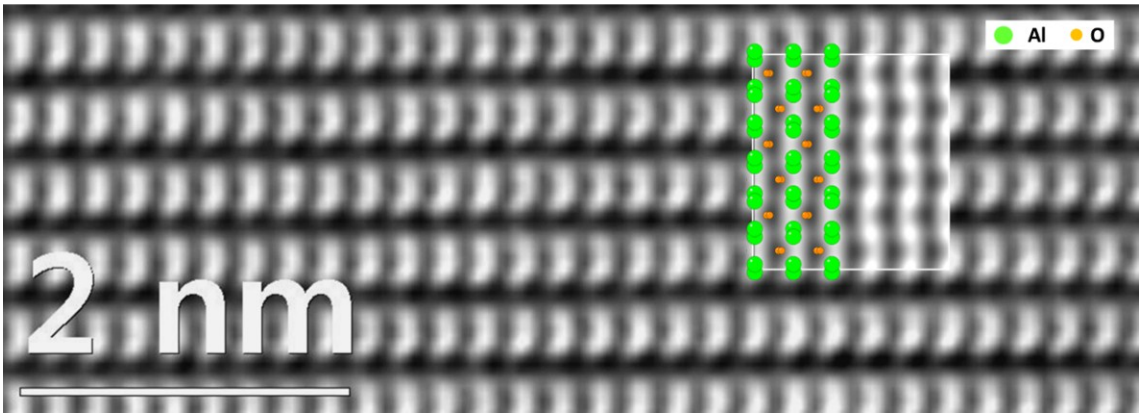

Figure S13. Microscope parameters used for the HRTEM image simulations that are chosen to approximate the experimental conditions as closely as possible. The bottom figure is a simulated image and consists of the corresponding atomic model superimposed on the experimental HRTEM image of sapphire (α-Al_2O_3) oriented to $[10\bar{1}0]$ direction.

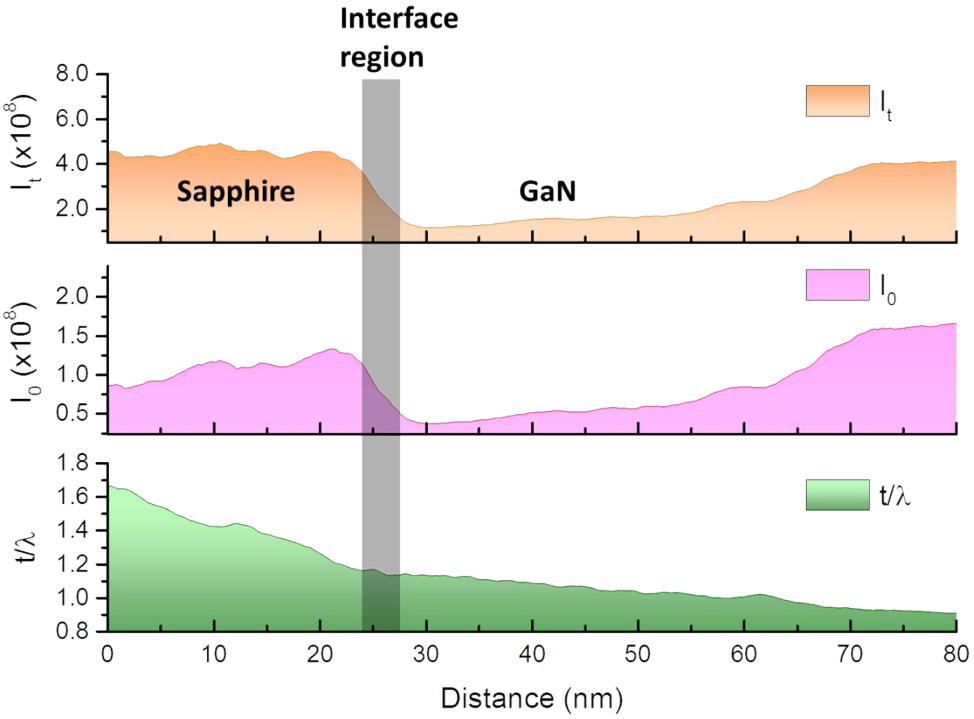

Figure S14. Measurement of the local relative thickness (*t*/λ) using the log-ratio formula, $t/\lambda = \ln(I_t/I_o)$, where t and λ are the thickness and electron wavelength, respectively, and I_t and I_o are the total and zero-loss intensities under EELS obtained across the GaN/sapphire interface, respectively. No variation in the resulting t/λ (green graph) is observed across the interface (see the area marked with the gray band). Thus, no preferential thinning (usually caused by different ion milling rates for thin films and substrates) occurred at the GaN/sapphire interface.